Simulation of salt cavity healing based on a micro-macro model of pressure-solution

Xianda Shen[1] & Chloé Arson[1]*

[1]*School of Civil and Environmental Engineering, Georgia Institute of Technology, Atlanta, GA 30332-0355*

**Corresponding author (e-mail: chloe.arson@ce.gatech.edu)*

Abstract: CO_2 storage in salt rock is simulated with the Finite Element Method (FEM), assuming constant gas pressure. The initial state is determined by simulating cavity excavation with a Continuum Damage Mechanics (CDM) model. A micro-macro healing mechanics model is proposed to understand the time-dependent behavior of halite during the storage phase. Salt is viewed as an assembly of porous spherical inclusions that contain three orthogonal planes of discontinuity. Eshelby's self-consistent theory is employed to homogenize the distribution of stresses and strains of the inclusions at the scale of a Representative Elementary Volume (REV). Pressure solution results in inclusion deformation, considered as eigenstrain, and in inclusion stiffness changes. The micro-macro healing model is calibrated against Spiers' oedometer test results, with uniformly distributed contact plane orientations. FEM simulations show that independent of salt diffusion properties, healing is limited by stress redistributions that occur around the cavity during pressure solution. In standard geological storage conditions, the displacements at the cavity wall occur within the five first days of storage and the damage is reduced by only 2%. These conclusions still need to be confirmed by simulations that account for changes of gas temperature and pressure over time. For now, the proposed modeling framework can be applied to optimize crushed salt back filling materials and can be extended to other self-healing materials.

The low permeability and self-healing potential of salt rock (halite) makes it a good potential host material for long-term geological storage, especially in wet conditions. So far, the actual use of salt formations for geological storage has been limited by technological challenges related to retrievability. However, in favorable stress, pore pressure and temperature conditions, salt stiffness and strength can indeed increase due to pressure solution, solid diffusion and recrystallization (Chan, et al. 1998; Tsang, et al. 2005; Zhu and Arson, 2015). Pressure solution is a very effective healing mechanism, common in crystalline media that contain water films, especially in halite. Salt minerals dissolve at contacts that are under high stress, diffuse along grain boundaries, and re-precipitate at pore walls, which are under lower stress (Paterson, 1973; Raj, 1982; Rutter, 1983). Based on thermodynamic equations established at the grain scale, experiments were conducted on granular salt and phenomenological models were proposed to predict healing in halite (Spiers et al., 1990; Yang et al., 1999; Houben et al., 2013). In this paper, we use a homogenization approach to understand the macroscopic effect of local pressure solution mechanisms at the scale of a Representative Elementary Volume (REV).

Eshelby's theory allows calculating the stress and strain fields of a REV made of an elastic matrix that contains ellipsoidal heterogeneities (Eshelby, 1957). Based on this theory, Mori and Tanaka proposed an explicit method to predict the homogenized stiffness of the REV, in which the interaction between the matrix and the inclusions is accounted for (Mori and Tanaka, 1973). However, when it is impossible to identify a dominating phase that can be considered as the matrix, like in polycrystalline materials, it is necessary to use a so-called self-consistent method (Kröner, 1961; Hill, 1965), in which the REV is seen as a juxtaposition of inclusions. Each inhomogeneity is seen as an inclusion embedded in a matrix that has the yet-unknown homogenized properties of the REV. Hence the properties of the matrix are not known *a priori*, which makes the model implicit. In what follows, we use a self-consistent method to upscale stresses and strains induced by local pressure solution. Since the time-dependent strains of the inclusions depend on thermodynamic processes that cannot be predicted from the far field stresses alone, we model local pressure solution strains as eigenstrains (e.g., Pichler and Hellmich, 2010). We then use our micro-macro model to simulate healing around salt cavities used for CO_2 storage.

We first explain the pressure solution phenomenon and we present the corresponding thermodynamic equations at the inclusion scale. Secondly, we formulate the micro-macro healing model based on a self-consistent homogenization scheme. We then calibrate the model against published experimental data. Lastly, we present Finite Element simulations of salt cavity healing during CO_2 storage.

Pressure solution model

Let us consider two halite crystals separated by a thin fluid film. A stress increase normal to the crystal boundary (called contact plane) leads to an increase of chemical potential ($\Delta\mu$) in the solid constituent in reference to the solute:

$$\Delta\mu=\sigma_e\Omega \quad (1)$$

where σ_e is the effective stress normal to the contact plane (defined as the difference between the normal stress and the fluid pressure) and Ω is the molar volume of NaCl (2.7×10^{-5} m^3 mol^{-1}). The drop of chemical potential in the solute can be expressed as a function of mineral concentration:

$$\Delta\mu = R^*T\ln(1+\frac{\Delta C}{C_o}) \quad (2)$$

where R^* is the gas constant, T is the Kelvin temperature and ΔC is the difference between the ionic concentration in the fluid films located at contact planes and that in the pores. C_0 is the reference concentration in the pores, located at crystals' edges (considered as sinks). Due to the difference of solute concentration between the contact planes and the pores, salt ions diffuse from high concentration sites (contact planes) to low concentration sites (pores). Figure 1 shows a schematic representation of the diffusion path around a pore. We define the elementary heterogeneity of salt rock as a hollow spherical inclusion that contains a pore located at the intersection of three orthogonal crystal contact planes (plane XY, plane YZ, and plane XZ in Figure 1). The salt crystals are assumed to be cubic with dimension of $2r_g$ (Overton and Swim, 1951; Zhang and Wu, et al. 2005). The diameter of grains of halite ranges between 0.01mm and several dm (Urai and Spiers, 2007; Urai and Schléder, et al. 2008). In this paper, we work with a grain dimension r_g of the order of 10^{-4} m, which is the typical size of salt crystals studied in the laboratory. This will make it possible to calibrate our model against reported experimental data in the sequel. The thickness of the solid wall around the pore is assumed to be uniform, so that the radius of an inclusion is equal to r_g. Noting W the thickness of the shell around the pore, the radius of the pore is r_g-W.

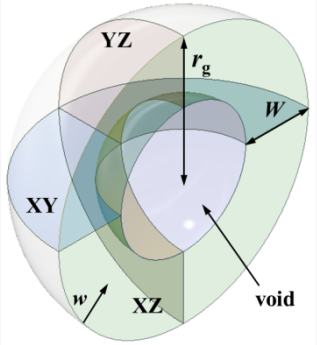

Figure 1. Schematic representation of the inclusion model

The pressure solution mechanism is illustrated in Figure 2. Salt dissolves at contact planes that are under high stress. We consider that pores act as sinks, so that ions diffuse towards the central pore and uniformly precipitate on the pore wall. The increase of pore wall thickness is noted δW.

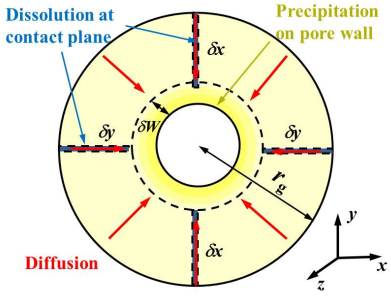

Figure 2. Pressure solution mechanism along contact plane XY

According to Fick's first law, the radial diffusion flux $J(w)$ along the contact plane is related to the diffusion coefficient D and the mineral concentration C as follows:

$$J(w) = -D\frac{\partial C}{\partial w} \quad (3)$$

where w is the distance between the periphery of the contact surface and the dissolution front, i.e., the wall thickness at a given time. The shape of the pore/film interface is an annulus, the area of which can be calculated as the product of

the film thickness, *S,* by the perimeter of the pore wall, $2\pi(r_g - w)$. The area of the contact plane between the periphery of the contact surface and the dissolution front is calculated as $(2r_g w - w^2)\pi$. Based on the principle of mass conservation, the total mass of mineral that diffuses towards the central pore is equal to the mass dissolved at the contact plane. Therefore:

$$J(w)2\pi\left(r_g - w\right)S = \frac{2V_c\left(2r_g w - w^2\right)\pi}{\Omega} \quad (4)$$

where V_c is the dissolution velocity. Pressure solution induces energy dissipation by diffusion. The energy dissipation per unit volume ($\dot{\Delta}_w$) can be calculated as (Lehner, 1990):

$$\dot{\Delta}_w = -J(w)\frac{\partial \mu}{\partial w} \quad (5)$$

The increment of radial energy dissipation is obtained by introducing Eq. 2, Eq. 3 and Eq. 4 in Eq. 5, and by integrating over the distance that goes from a point at the periphery of the inclusion to the pore wall. It is assumed that the solute concentration at grain boundaries, $C(w)$, is equal to the solute concentration in the pores (C_o) (Rutter,1983; Schutjens and Spiers, 1999; Pluymakers and Spiers, 2015). The total energy dissipated along the contact plane XY is obtained as:

$$\dot{\Delta}^{XY} = \int_0^W \frac{2R^*TV_{XY}^2\pi\left(2r_g w - w^2\right)^2}{DC_0 S\Omega^2\left(r_g - w\right)}dw \quad (6)$$

where V_{xy} is the dissolution velocity on the plane XY. We assume that the total input work at a contact plane is entirely dissipated by diffusion. The velocity V_{xy} can thus be calculated as:

$$V_{XY} = \frac{DC_o S\Omega^2\sigma_{XY}^e\left(2r_g W - W^2\right)}{R^*T\int_0^W \frac{\left(2r_g w - w^2\right)^2}{r_g - w}dw} \quad (7)$$

where σ_{XY}^e is the effective stress normal to the contact plane XY. With the expression of the dissolution velocity, we obtain the inclusion strain rate and the change of pore wall thickness, as follows:

$$\dot{\gamma}_z = \frac{V_{XY}}{r_g} \quad (8)$$

$$\dot{W} = \frac{V_{XY} + V_{YZ} + V_{XZ}}{A_s} \quad (9)$$

where A_s is the surface area of the pore in the center of the inclusion, and γ_z is the chemical strain.

Homogenization scheme

In order to predict the stiffness, deformation and stress of salt rock at the REV scale, a self-consistent homogenization scheme is adopted. The strain of a spherical inclusion can be expressed as (Dvorak and Benveniste, 1992):

$$\varepsilon^i = A^i : E + \sum_{j=1}^{n} D^{ij} : \gamma^j \quad (10)$$

where ε^i and A^i are the strain and concentration tensors of inclusion *i*, respectively; *n* is the total number of inclusions in the REV (characterized by their porosity and plane orientations); D^{ij} is the influence tensor of inclusion *j* on inclusion *i*;

γ^j is the eigenstrain of inclusion j (the chemical strain induced by pressure solution); E is the strain of REV. Based on Eshelby's inclusion-matrix theory, the concentration tensor A^i can be calculated as (Dormieux et al, 2006):

$$A^i = \left[I + P^i : \left(C^i - C^h\right)\right]^{-1} : \left\{\sum_{j=1}^{n} \varphi^j \left[I + P^j : \left(C^j - C^h\right)\right]^{-1}\right\}^{-1} \quad (11)$$

where φ_i is the volume fraction of inclusion i in the REV, P^i is the P tensor (also called Hill's tensor in some references), C^i is the stiffness of inclusion i, and C^h is the homogenized stiffness of the REV. P^i is a fourth order tensor that depends on the shape of the inclusion and on the stiffness of the REV. The explicit expression of the P tensor was given by Mura (1987). C^i is calculated based on a damage model, to be determined. Two examples of such damage models will be given, one at lab scale for calibration and verification purposes, and one at cavity scale for numerical simulations. The homogenized stiffness C^h can be calculated implicitly, as follows:

$$C^h = \sum_{i=1}^{n} \varphi^i C^i : A^i \quad (12)$$

For spherical inclusions, the influence tensors D^{ij} are expressed as follows (Pichler and Hellmich, 2010):

$$D^{ii} = \left(I - \left(\varphi^i A^i\right)\right) : \left[I + P^i : \left(C^i - C^h\right)\right]^{-1} : P^i : C^i \quad (13)$$

$$D^{ij} = -\varphi^j A^i : \left[I + P^j : \left(C^j - C^h\right)\right]^{-1} : P^j : C^j \quad (14)$$

Note that influence tensors have a more complex form for ellipsoidal inclusions. The stress of the inclusion depends on the stiffness, chemical strain and total strain of the inclusion, as follows:

$$\sigma^i = C^i : \left(\varepsilon^i - \gamma^i\right) \quad (15)$$

In a strain-controlled numerical simulation, at a given time t, the strain of the REV (E_t), the chemical strain γ_t^i of each inclusion, and the stiffness of each inclusion are known. The homogenized stiffness C_t^i is calculated iteratively, from Eq.11 and Eq.12. Substituting Eq.13 and Eq.14 into Eq.10, the local strain ε_t^i is determined. The local stress of each inclusion is then obtained from Eq.15. The chemical strain γ_{t+1}^i and the porosity of the inclusions are updated incrementally by using Eq.8 and Eq.9.

Calibration against oedometer test results

We first applied our model at laboratory scale. We closed the formulation by introducing a damage model at inclusion scale. In granular materials, the shear modulus depends on porosity (Kováčik, 2008) and increases with the hydrostatic stress (Digby, 1981). Accordingly, for each inclusion, we assumed that the shear modulus μ^* was related to the porosity of the inclusion ϕ and to the effective stress σ_e, as follows:

$$\mu^* = \eta\left(1-\phi\right)^m \sigma_e^n \quad (16)$$

where η, m and n are constants that need to be calibrated. Note that η, m and n are assumed to be the same for all inclusions. μ^* and ϕ are inclusion-specific (but the i index was dropped in Eq.16 for clarity). The stiffness of inclusion i is expressed as:

$$C^i = \frac{2\mu^* \upsilon}{1-2\upsilon} \boldsymbol{I} \otimes \boldsymbol{I} + 2\mu^* \delta \quad (17)$$

where $\boldsymbol{I}$ is the second-rank identity tensor, and δ is the symmetric part of the fourth-rank identity tensor.

We simulated oedometer tests conducted by Spiers' group on saturated granular salt (Spiers, et al. 1993). The micro-macro model presented above was implemented in a Finite Element Method (FEM) package and simulations were done with only one element, to reflect the behavior at the material point. In conformity with the experiments, the crystal and void size distributions were assumed uniform in the REV, with an initial porosity of 42%, and a crystal size of r_g=0.1375mm (equal to the inclusion size in our microstructure model). We assumed that the distribution of contact plane orientations was uniform. Numerical creep curves were fitted to the experimental results obtained under compressions of -8.0MPa, -4.2MPa and -1.1MPa (Figure 3). The corresponding calibrated parameters are reported in Table 1. We define the prediction error as the difference between the area below the experimental creep curve and the area below the numerical creep curve, normalized by the area below the experimental creep curve. The errors made in the numerical predictions are 5.7%, 4.0%, and 3.7% for oedometer tests under -8.0MPa, -4.2MPa and -1.1MPa, respectively.

Table 1 Parameters used to simulate oedometer tests

Chemical parameters			Elastic parameters		
DS	C_0	T	η	m	n
2.0×10^{-7} mm^3	0.163 m^3/m^3	22 ^{o}C	8.4	0.2	0.64

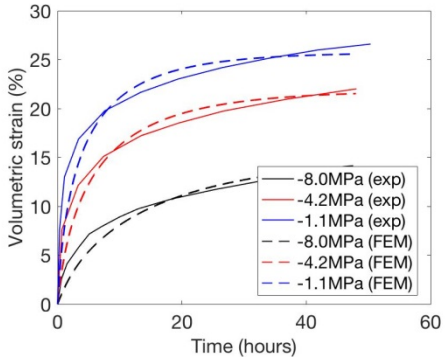

Figure 3. Calibration of the micro-macro healing model against oedometer test results

During the oedometer tests, the creep rate decreases due to: (i) *The increase of the diffusion path length in each inclusion*: precipitation at the pore wall increases the migration distance of the ions from the periphery of the inclusion to the pore wall; (ii) *The decrease of compressive stress at inclusion and REV scales*: during pressure solution, the dimensions of the inclusions decrease in the directions normal to the contact planes where dissolution occurs; according to Eq. (7) and Eq. (8), compressive stress at contact planes is relaxed, which leads to smaller chemical potential differences between the solid and the solute, hence less dissolution.

Simulation of CO_2 storage in a salt cavern

Secondly, we applied our model at cavity scale. We closed the formulation by introducing a damage model at REV scale. The FEM is used to simulate CO_2 storage in a salt cavern. Based on the work of Dusseault (2004), the salt cavern is modeled as an oblate spheroid with a vertical axis of 100m and horizontal axes of 150m. The centroid of the cavern is located at a depth of 1,200m and halite density is taken equal to 2,400kg/m^3. After excavation, the cavern is sealed at a pressure of 15MPa. The FEM model's dimensions are 1650m×375m×375m (Figure 4). The lateral displacement of salt rock at the external boundary is fixed. We used a Continuum Damage Mechanics (CDM) model (described below)

to simulate the excavation phase. In a second stage, the micro-macro healing model presented above was used to simulate the storage phase, by applying a 15MPa pressure at the cavern wall. Note that the incremental relation is obtained by a local homogenization and upscaling method and not through a macroscopic law previously established. The initial value of porosity in the healing simulation phase is set equal to the value of the damage variable W^* calculated after the excavation phase. During the storage phase, porosity decreases due to pressure solution, which is expected to increase halite stiffness – a process referred to as "self-healing". We first performed a mesh sensitivity analysis. Results confirmed that mesh size only influence the damage value after the excavation phase, but has very little effects on the predicting of healing.

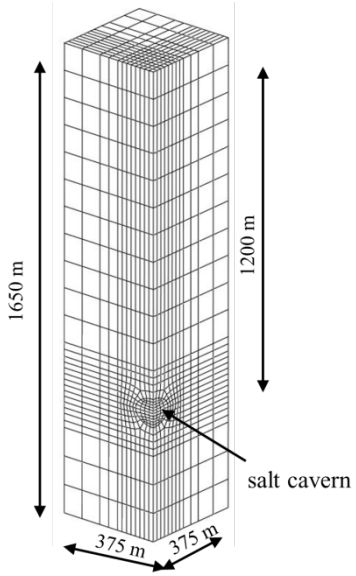

Figure 4. Dimensions and mesh of the FEM model

A thermodynamics based CDM model is used to predict excavation damage. At REV scale, the expression of Helmholtz free energy Ψ_s is given as (Halm and Dragon, 1998; Zhu and Arson, 2015):

$$\Psi_s = \frac{1}{2}\lambda_o\left(\mathrm{tr}\varepsilon\right)^2 + \mu_o \mathrm{tr}\left(\varepsilon\cdot\varepsilon\right) + \alpha \mathrm{tr}\varepsilon \mathrm{tr}\left(\Omega^*\varepsilon\right) + 2\beta \mathrm{tr}\left(\Omega^*\varepsilon\cdot\varepsilon\right) \quad (18)$$

where λ_o and μ_o are Lamé constants; α and β are damage material parameters; Ω^* is the dimensionless damage variable, considered as a scalar porosity in the present study. The damage driving force Y_d is expressed from thermodynamic conjugation relationships, as follows:

$$Y_d = -\frac{\partial \Psi_s}{\partial \Omega^*} = -\alpha \mathrm{tr}\varepsilon \mathrm{tr}\varepsilon - 2\beta \mathrm{tr}\left(\varepsilon\cdot\varepsilon\right) \quad (19)$$

The damage criterion is expressed as:

$$f_d = \frac{Y_d}{\sqrt{2}} - \left(k_o + k_1\Omega^*\right) \quad (20)$$

where k_o is the damage initiation threshold and k_1 a damage hardening parameter. During the initiation and propagation of damage, the consistency conditions hold (i.e., f_d=0 and δf_d=0). The damage parameters used for the simulation, taken from a prior study (Zhu and Arson, 2015), are reported in Table 2.

Table 2 Damage parameters used for the excavation simulation

λ_o	μ_o	α	β	k_o	k_1
2.64×10^{10} Pa	1.75×10^{10} Pa	1.90×10^{9} Pa	-2.04×10^{10} Pa	1000 Pa	2.50×10^{5} Pa

Figure 5 shows the distribution of damage around the salt cavern after excavation. The maximum damage observed reaches 9.8% and appears in the middle of sidewall, due to the high compressive principal stress. Damage drops rapidly away from the cavern wall. The size of the damage zone is of the order of the cavern's radius.

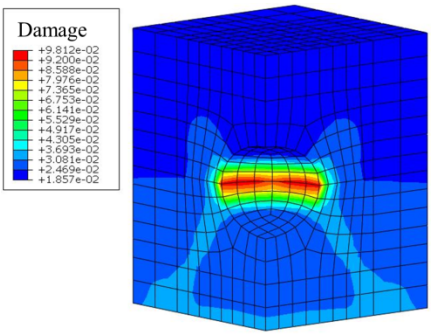

Fig. 5 Halite damage after excavation

In a second step, we use the micro-macro healing model with randomly oriented inclusions to simulate the storage phase. The REV porosity is calculated from the porosity of the inclusions, and used as the damage variable in the expression of REV stiffness that derives from the expression of the free energy in the CDM model above (Eq.17). The minimum (compressive) principal stress distribution around the cavern is represented in Figure 6, for $DS = 1.0\times10^{-18}$ m^3 and r_g=0.13mm. The corresponding evolution of damage at the cavern wall is shown in Figure 7. The evolution of cavity convergence is illustrated in Figure 8.

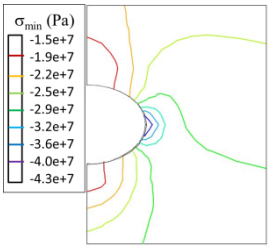

(a) Just after excavation (no healing time)

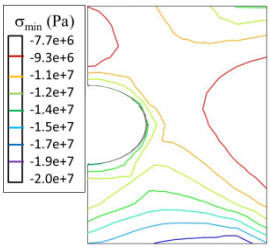

(b) After 100 hours of storage (100 hours of healing)

Figure 6. Minimum (compressive) principal stress distribution around the cavity (zone of dimensions 225m×300m).

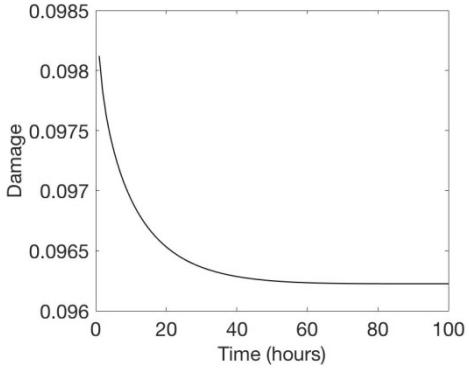

Figure 7. Evolution of damage at the cavern wall during the storage phase

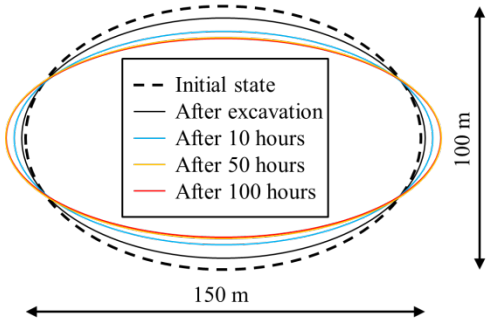

(a) Evolution of the cavity shape (magnified 200 times)

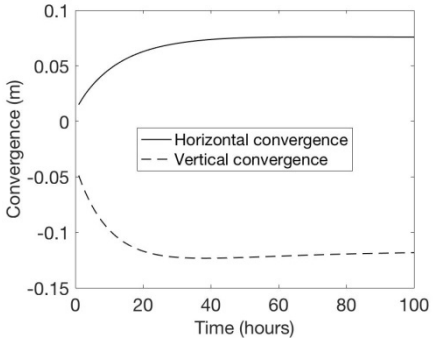

(b) Evolution of horizontal and vertical convergences during storage

Figure 8. Evolution the deformation of the salt cavern during storage

Figure 6 clearly shows that the compressive principal stress decreases over time during the storage phase. This is because the dissolution of salt at contact planes triggers negative chemical strains at the inclusion scale. Since halite elements are geometrically constrained, inclusion shrinkage results in tensile stresses at the REV scale, which reduce the overall compressive stresses around the cavern. The decrease of compressive stress is particularly visible in the elements with large initial damage in the middle of the sidewall, where the compressive principal stress switches from -43MPa after excavation to -15MPa during storage. Figure 7 confirms that stress redistribution at the cavern wall is due to healing, i.e., to the reduction of damage, defined here as porosity. Because pressure solution relaxes compressive stress at the contact planes, the dissolution rate decreases over time as salt precipitation occurs at the pore walls. In other words, healing is self-limited. As a result, the healing rate decreases rapidly during the three first days of storage, after which damage reaches a plateau. At the sidewall, damage amounts to 9.8% after excavation, and to 9.6% after

four days of storage. Healing thus reduced the maximum damage by 2%. Just after excavation, the vertical convergence is -0.048m, and the horizontal convergence is +0.015m (see Figure 8). Pressure solution increases convergence, which reaches 1% in both horizontal and vertical directions after four days of storage. Cavern deformation stabilizes when healing reaches a plateau.

Figure 9 presents a sensitivity analysis of the parameter *DS*, which is the product of the diffusion coefficient (*D*) by the thickness of the fluid films at contact planes (*S*). Clearly, the healing rate increases with *DS*, which can be seen as a diffusive efficiency parameter. Physically, pressure solution occurs faster when the diffusion coefficient is higher and/or when the inter-crystalline space is larger. However, *DS* does not influence the final damage value at the cavity wall, because the rate of pressure solution is independent of the stress redistributions that occur around the cavern (Figure 9(a)). Similarly, a high diffusive efficiency accelerates convergence but does not influence the final shape of the storage facility (Figure 9(b)).

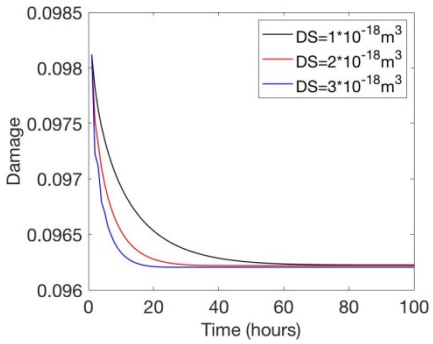

(a) Damage evolution

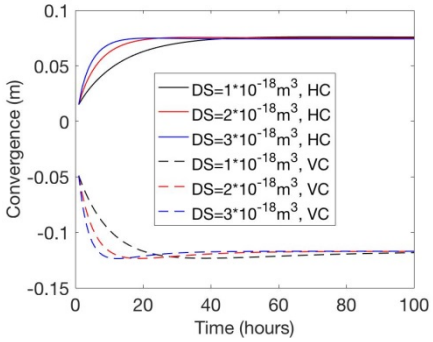

(b) Convergence development

Figure 9. Effect of diffusive efficiency on cavern healing

Figure 10 illustrates the influence of the size of the inclusions on salt healing. Inclusion size is equivalent to crystal size and indicates how long the diffusion path is, from high stress dissolution sites to low stress precipitation sites. Larger inclusions imply longer diffusion paths thus lower healing rate. At same initial porosity, larger inclusions also mean fewer inclusions. After 2 days of storage, healing with a crystal size of 0.26mm is only 50% of the healing obtained with a crystal size of 0.13mm, and the asymptotic values of damage and convergence are reached after 20 days. The healing rate is negligible with a crystal size of 1.30mm, which shows that the healing rate is more sensitive to the crystal size than to the diffusive efficiency.

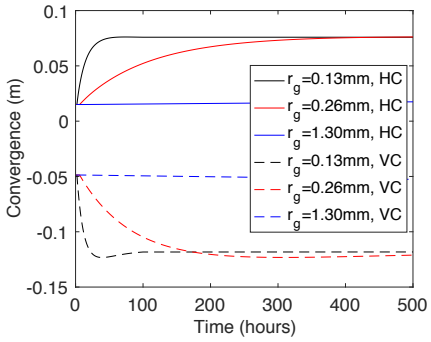

(a) Damage evolution

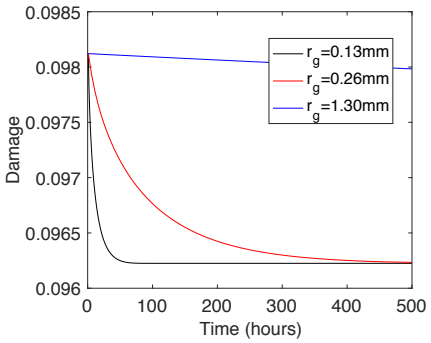

(b) Convergence development

Figure 10. Effect of inclusion radius on cavern healing

Conclusions

In this paper, we propose a micro-macro healing mechanics model that captures the effect of pressure solution on halite porosity. Thermodynamic equations of pressure solution are established at the scale of an inclusion defined as a hollow sphere intersected by three orthogonal contact planes that contain a fluid film. Stress at the contact planes determines the dissolution rate. The pore at the center of the inclusion is viewed as a sink: ions diffuse from the dissolution sites to the pore wall, where they precipitate. The resulting rate of deformation of the inclusion is calculated from mass balance equations, and then defined as an eigenstrain in a self-consistent homogenization scheme. The micro-macro healing model is calibrated against published oedometer test results and implemented in a FEM package.

CO_2 storage in a deep oblate spheroidal salt cavity is simulated. A continuum damage model is used to calculate the damage induced by excavation. The micro-macro healing model is used to simulate the storage phase under constant gas pressure. In real storage conditions, gas pressure increases due to convergence. However, in the present study, convergence was limited to an asymptotic value of 1%, which was not found to influence gas pressure. Due to the healing process, stress around the salt cavern is redistributed and becomes uniform. The largest compressive principal stress is decreased by 65%. Under these conditions, numerical calculations show that only 2% of the excavation damage can be recovered at the sidewall, where damage is the highest. Damage and convergence reach a plateau after four days of storage. The healing rate decreases over time because (i) Salt precipitation at pore walls lengthens the diffusion path of the ions dissolved at high compression stress sites; (ii) Healing results in a stress redistribution around the cavity, reducing compressive stresses, thus limiting the triggering of pressure solution. Higher diffusion coefficients and thicker fluid films can accelerate healing, but cannot change its asymptotic value. A larger crystal size significantly

decreases the healing rate.

Simulation results indicate limited healing potential around salt cavities used for CO_2 storage, but it has to be noted that the healing model was calibrated at laboratory scale for a uniform size distribution of crystals, which is not representative of realistic storage conditions. In addition, temperature effects were left out in this study. In future work, we will study the effect of grain size distribution and we will formulate a more comprehensive damage and healing thermo-hydro-mechanical model. As is, the proposed modeling framework can be used to optimize some microstructure parameters of crushed salt buffers (such as porosity and fluid inclusion distribution) and it can be extended to other self-healing materials.

Acknowledgements

This work was supported by the U.S National Science Foundation, under grant CMMI#1552368: "CAREER: Multiphysics Damage and Healing of Rocks for Performance Enhancement of Geo-Storage Systems - A Bottom-Up Research and Education Approach."

References

Chan, K.S., Bodner, S.R., Munson, D.E. 1998. Recovery and Healing of Damage in WIPP Salt, International Journal of Damage Mechanics, 7, 143-166.

Digby, P., 1981. The effective elastic moduli of porous granular rocks. Journal of Applied Mechanics 48 (4), 803-808.

Dormieux, L., Kondo, D., and Ulm, F.-J. 2006. Microporomechanics, Wiley, New York.

Dusseault, M.B. & Bachu, S. & Rothenburg, L., 2004. Sequestration of CO_2 in Salt Caverns. Journal of Canadian Petroleum Technology, 43(11), 49-55.

Dvorak, G. J. 1992. "Transformation field analysis of inelastic composite materials." Proc. R. Soc. London, Ser. A, 437, 311–326.

Eshelby, J. D., 1957. The determination of the elastic field of an ellipsoidal inclusion, and related problems. Proceedings of the Royal Society of London A: Mathematical, Physical and Engineering Sciences 241 (1226), 376-396.

Hill, R., 1965. Continuum micro-mechanics of elastoplastic polycrystals. Journal of the Mechanics and Physics of Solids 13 (2), 89-101.

Houben, M., Hove, A., Peach, C., Spiers, C., 2013. Crack healing in rocksalt via diffusion in adsorbed aqueous films: Microphysical modelling versus experiments. Physics and Chemistry of the Earth, Parts A/B/C 64 (Supplement C), 95 -104, coupled Physical and Chemical Transformations Affecting the Performance of GeoSystems.

Kováčik, J., 2008. Correlation between elastic modulus, shear modulus, poisson's ratio and porosity in porous materials. Advanced Engineering Materials 10 (3), 250-252.

Kröner, E., 1961. Zur plastischen verformung des vielkristalls. Acta Metallurgica 9 (2), 155-161.

Halm D, Dragon A (1998) An anisotropic model of damage and frictional sliding for brittle materials. Eur J Mech Solids 17(3):439–460

Lehner, F. K., 1995. A model for intergranular pressure solution in open systems. Tectonophysics 245 (3-4), 153-170.

Mori, T., Tanaka, K., 1973. Average stress in matrix and average elastic energy of materials with misfitting inclusions. Acta Metallurgica 21 (5), 571-574.

Mura, T. 1987. Micromechanics of defects in solids, Martinus Nijhoff Publishers, Dordrecht.

Paterson, M. S., 1973. Nonhydrostatic thermodynamics and its geologic applications. Reviews of Geophysics 11 (2), 355-389.

Pluymakers, A. M. H., Spiers, C. J., 2015. Compaction creep of simulated anhydrite fault gouge by pressure solution: theory v. experiments and implications for fault sealing. Geological Society, London, Special Publications 409 (1), 107-124.

Pichler, B. and Hellmich, C. 2010. Estimation of influence tensors for eigenstressed multiphase elastic media with nonaligned inclusion phases of arbitrary ellipsoidal shape, Journal of engineering mechanics, vol. 136, no. 8, 1043–1053.

Raj, R., 1982. Creep in polycrystalline aggregates by matter transport through a liquid phase. Journal of Geophysical Research: Solid Earth 87 (B6), 4731-4739.

Rutter, E. H., 1983. Pressure solution in nature, theory and experiment. Journal of the Geological Society 140 (5), 725-740.

Schutjens, P., Spiers, C., 1999. Intergranular pressure solution in NaCl: Grain-to-grain contact experiments under the optical microscope. Oil & Gas Science and Technology 54 (6), 729-750.

Spiers, C. J., Schutjens, P. M. T. M., Brzesowsky, R. H., Peach, C. J., Liezenberg, J. L., Zwart, H. J., 1990. Experimental determination of constitutive parameters governing creep of rocksalt by pressure solution. Geological Society, London, Special Publications 54 (1), 215-227.

Spiers, C., Brzesowsky, R., 1993. Densification behavior of wet granular salt: Theory versus experiment. In: Seventh Symposium on salt. Vol. 1, 83-92.

Tsang, C.F., Bernier, F., Davies, C., 2005. Geohydromechanical processes in theExcavation Damaged Zone in crystalline rock, rock salt, and indurated and plasticclays-in the context of radioactive waste disposal. Int. J. Rock Mech. Min. Sci. 42 (1), 109–125.

Yang, C., Daemen, J., Yin, J.-H., 1999. Experimental investigation of creep behavior of salt rock. International Journal of Rock Mechanics and Mining Sciences 36 (2), 233-242.

Zhu, C. & Arson C., 2015. A model of damage and healing coupling halite thermomechanical behavior to microstructure evolution", Geotechnical and Geological Engineering, 33(2), 389–410.